Bull Volcanol (2000) 61:477–490

ORIGINAL PAPER

T. Brombach · L. Marini · J. C. Hunziker

Geochemistry of the thermal springs and fumaroles of Basse-Terre Island, Guadeloupe, Lesser Antilles

Received: 9 November 1998 / Accepted: 15 July 1999

Abstract The purpose of this work was to study jointly the volcanic-hydrothermal system of the high-risk volcano La Soufrière, in the southern part of Basse-Terre, and the geothermal area of Bouillante, on its western coast, to derive an all-embracing and coherent conceptual geochemical model that provides the necessary basis for adequate volcanic surveillance and further geothermal exploration. The active andesitic dome of La Soufrière has erupted eight times since 1660, most recently in 1976–1977. All these historic eruptions have been phreatic. High-salinity, Na–Cl geothermal liquids circulate in the Bouillante geothermal reservoir, at temperatures close to 250 °C. These Na–Cl solutions rise toward the surface, undergo boiling and mixing with groundwater and/or seawater, and feed most Na–Cl thermal springs in the central Bouillante area. The Na–Cl thermal springs are surrounded by Na–HCO_3 thermal springs and by the Na–Cl thermal spring of Anse à la Barque (a groundwater slightly mixed with seawater), which are all heated through conductive transfer. The two main fumarolic fields of La Soufrière area discharge vapors formed through boiling of hydrothermal aqueous solutions at temperatures of 190–215 °C below the "Ty" fault area and close to 260 °C below the dome summit. The boiling liquid producing the vapors of the Ty fault area has δD and δ^{18}O values relatively similar to those of the Na–Cl liquids of the Bouillante geothermal reservoir, whereas the liquid originating the vapors of the summit fumaroles is strongly enriched in ^{18}O, due to input of magmatic fluids from below. This process is also responsible for the paucity of CH_4 in the fumaroles. The thermal features around La Soufrière dome include: (a) Ca–SO_4 springs, produced through absorption of hydrothermal vapors in shallow groundwaters; (b) conductively heated, Ca–Na–HCO_3 springs; and (c) two Ca–Na–Cl springs produced through mixing of shallow Ca–SO_4 waters and deep Na–Cl hydrothermal liquids. The geographical distribution of the different thermal features of La Soufrière area indicates the presence of: (a) a central zone dominated by the ascent of steam, which either discharges at the surface in the fumarolic fields or is absorbed in shallow groundwaters; and (b) an outer zone, where the shallow groundwaters are heated through conduction or addition of Na–Cl liquids coming from hydrothermal aquifer(s).

Key words Fluid geochemistry · Thermal springs · Fumaroles · Guadeloupe · Geothermal · Volcano

Editorial responsibility: D. A. Swanson

Tatjana Brombach (✉) · Johannes C. Hunziker
Université de Lausanne, Institut de Minéralogie et Pétrographie, BFSH2, CH-1015 Lausanne, Switzerland

Luigi Marini
Dipartimento di Scienze della Terra, Università di Genova, Corso Europa 26, I-16132 Genova, Italy

Introduction

Basse-Terre, the western Island of Guadeloupe, is in the middle of the Lesser Antilles active island arc. It consists of different volcanic-structural units. The Madeleine-Soufrière unit is the most recent and contains the presently active dome of La Soufrière volcano. This andesitic dome was built ~500 BP, and only phreatic activity has been recorded since then, with one of the most violent eruptions between 1976 and 1977 (Westercamp and Tazieff 1980). Similar phreatic eruptions have the highest probability of recurrence (Boudon et al. 1987).

Thermal manifestations are concentrated mainly around La Soufrière dome and in the Bouillante geothermal area (Fig. 1). Two thermal springs in the northern part of the island are not included in this study. Many geothermal features of Bouillante were described during early surface exploration but have disappeared by now, probably due to the exploitation of the geothermal system. The hottest thermal spring of Bouil-

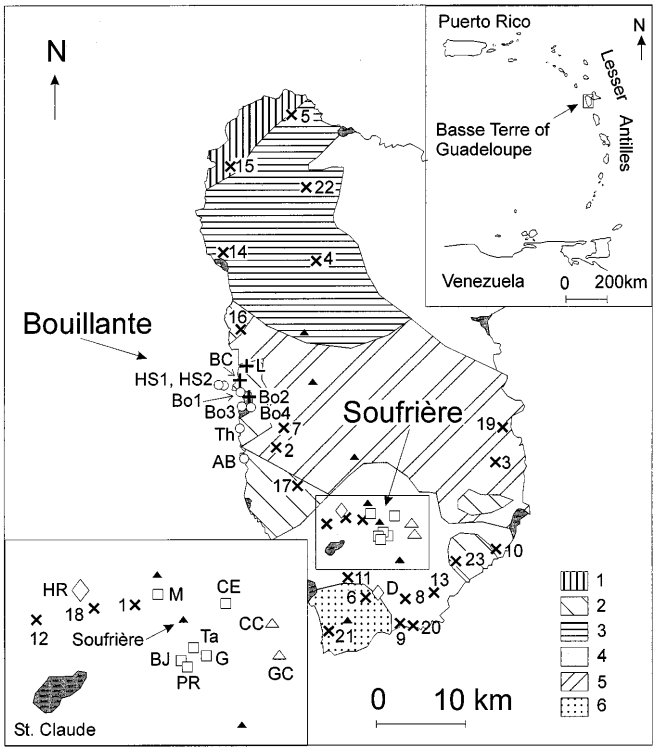

Fig. 1 Map of Basse Terre showing the location of cold springs (*crosses*), Na–Cl waters (*circles*), Na–HCO_3 waters (*plus symbols*), Ca–SO_4 waters (*squares*), Ca–Na–Cl waters (*triangles*), Ca–Na–HCO_3 waters (*diamonds*). Geology: *1* Basal Volcanic Complex (>3.5 Ma); *2* Bouillante Chain volcanism (0.8/0.6–0.2 Ma); *3* Northern Chain volcanism (3.5?–1.0 Ma); *4* Madeleine-Soufrière andesitic massif (<0.2 Ma); *5* Axial Chain volcanism (1.0–0.6 Ma); *6* Monts Caraibes volcanism (0.5 Ma). The *filled triangles* indicate the summits. Geology after Bouysse et al. (1985)

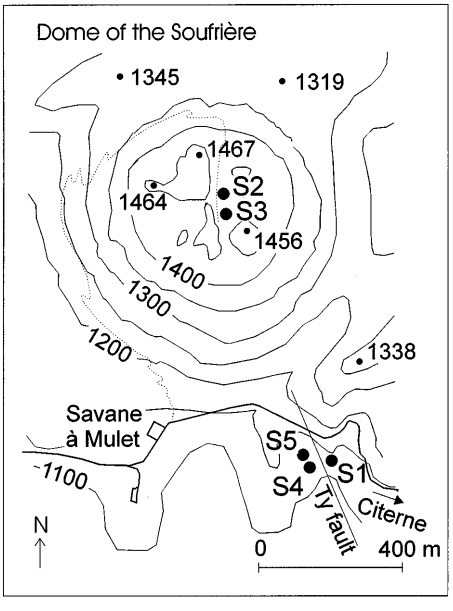

Fig. 2 Location of sampled fumaroles (*filled circles*) at the dome of La Soufrière

lante now has an outlet temperature of 74 °C, but a hydrothermal spring (HS2), which was sampled at 23 m under sea level by Traineau et al. (1997), reaches 92 °C. Low-pressure steaming ground also occurs at Bouillante.

A major vent system is at the top of La Soufrière dome, around which some smaller fumaroles occur. Another fumarolic field is present approximately 300 m below the top, at the southeastern foot of the dome, in the "Ty" fault area (Fig. 2). The few active fumaroles of this lower fumarolic field are the remnants of a much larger, heavily self-sealed fumarolic field, as indicated by the presence of widespread advanced argillic alteration.

In the 1970s four geothermal wells were drilled to depths of 350–2500 m during the exploration phase of the Bouillante geothermal field. They show anisotropic permeability distribution, rendering the exploitation of the system difficult (Demians D'Archimbaud and Surcin 1976). Only one well (B2) is presently used for production, operating a 4.7-MW geothermal power plant. It has a maximum temperature of 245 °C at 400 m and discharges a Na–Cl aqueous solution with Cl content of ~11,700 mg/kg under reservoir conditions (Traineau et al. 1997).

Until now the geothermal area of Bouillante and the thermal features of Soufrière Volcano were generally studied separately. The geothermal field of Bouillante was studied intensively by Cormy et al. (1970), Demians D'Archimbaud and Surcin (1972, 1976), and Traineau et al. (1997). The thermal springs of La Soufrière were studied by Pascaline (1980) and Benauges (1981).

We undertook a geochemical study of the complete suite of fluids encountered in Basse-Terre, integrating available data with the results of a geochemical survey carried out in 1997, in order to study the integral volcanic-hydrothermal system of Guadeloupe Island. Geothermal systems located along convergent plate boundaries generally receive inputs of magmatic fluids, even if they occur peripheral to active volcanoes. In particular, the contribution of andesitic magmatic water is clearly demonstrated by the δD and δ^{18}O values of geothermal waters (Giggenbach 1992a) and the presence of acid liquids in some geothermal systems, e.g., at Miravalles, Costa Rica (Giggenbach and Corrales Soto 1992). Shallow hydrothermal systems are frequently present below or close to active craters, such as at Nevado del Ruiz, Colombia (Giggenbach et al. 1990); Nisyros, Greece (Marini et al. 1993; Chiodini et al. 1993); Guagua Pichincha, Ecuador (Marini et al. 1991); Montserrat, West Indies (Chiodini et al. 1996); and Galeras, Colombia (Fischer et al. 1997). The small, shallow hydrothermal system identified at Galeras Volcano (Fischer et al. 1997; Sano et al. 1997), and the hydrothermal system at Nevado del Ruiz (Giggenbach et al. 1990), gave a comparatively quick response to the changes in volcanic activity before an impending eruption. However, there was no phreatic (hydrothermal) explosion of any

kind prior to the eruption. Phreatic activity characterized the incipient reactivation of the volcanic (magmatic) system and was followed by magmatic activity at Montserrat (Chiodini et al. 1996), whereas phreatic events took place at La Soufrière (Westercamp and Tazieff 1980), Guagua Pichincha (Marini et al. 1991), and Nisyros (Marini et al. 1993; Chiodini et al. 1993), but were not followed by any magmatic eruption. Due to this complex behavior, all volcanic-hydrothermal systems along convergent plate boundaries should be investigated through an integrated approach, both for geothermal exploration and volcanic surveillance.

Field observations, sampling, and analytical methods

Water samples from 25 thermal springs, 25 cold springs, and local seawater were collected during the 1997 geochemical survey. Most of the thermal springs have very weak flow rates, between 0.01 and 1 kg/s. The thermal springs Carbet Echelle, Bains Jaunes, Habitations Revel, and Galion of La Soufrière area have higher flow rates, reaching several kilograms per second, and the thermal springs of Matouba and Dolé have flow rates of approximately 100 kg/s. Raw, filtered (0.45 μm) and filtered-acidified (with HNO_3) aliquots were collected in polyethylene bottles for the determination of chemical constituents. Filtered aliquots were stored in glass bottles for isotope analyses. Outlet temperature, pH, alkalinity (by titration with HCl 0.1N using methylorange as indicator), and electric conductivity were measured in the field. Major ions were analyzed by ion chromatography (Dionex DX 300), trace elements and silica by ICP-MS.

Fumarolic fluids were collected from the top of La Soufrière dome (samples S2 and S3) and in the Ty fault area (samples S1, S4, and S5; Fig. 2). The outlet temperatures of all the sampled fumaroles (94–95 °C) are close to the boiling point of pure water at the average atmospheric pressure (850–880 mbar) of their discharge elevation (1150–1460 m above sea level, a.s.l.). The following samples were collected at these five sites: (a) total fluids in evacuated flasks containing 4 M NaOH solution, for the determination of most chemical constituents; (b) steam condensates (for the determination of the D/H and $^{18}O/^{16}O$ ratios of H_2O) and dry gases (for CO measurement), by passing the fumarolic fluids through an ice-bath condenser. In addition, the steam condensate and dry gases were also sampled from the low-pressure steaming ground of Bouillante. Gas constituents were analyzed at the Institute of Geochronology and Isotope Geochemistry of CNR, Pisa (Italy), following the methodology by Cioni et al. (1980) and Cioni and Corazza (1981). Carbon monoxide was measured in the incondensable gases by means of a gas-chromatograph fitted with a reduced gas detector (HgO).

The isotopic ratios were determined using a Finnigan MAT 251 (Finnigan, Bremen, Germany) mass spectrometer, calibrated with an internal standard "INHOUSE," which is calibrated against SMOW and SLAP international reference materials and GISP intercalibration material following the recommendation of Coplen (1988). For the determination of the δD value, water was converted to H_2 by reduction with Cr, whereas the $\delta^{18}O$ was measured on CO_2 previously equilibrated with water. Deviation of the intra-laboratory INHOUSE standard is ± 0.05‰ for $\delta^{18}O$ and ± 1‰ for δD.

Analytical results are reported in Tables 1 and 2.

Water chemistry

Thermal waters can be divided into the following hydrochemical types, on the basis of relative Na, Ca, and Mg contents (Fig. 3a) and relative Cl, SO_4, and HCO_3 concentrations (Fig. 3b): Na–Cl, Na–HCO_3, Ca–SO_4, Ca–Na–Cl, and Ca–Na–HCO_3 waters.

The first two water types are restricted to the Bouillante area; both have neutral to slightly alkaline pH values. The Na–Cl waters are characterized by generally high mineral contents (TDS up to 30,000 mg/kg) and high discharge temperatures (34–74 °C, up to 92 °C for spring HS2). This water type includes the geothermal liquids discharged by the wells B2 and B4, the submarine springs HS1 and HS2 at 10 and 23 m depth (data from Traineau et al. 1997), and the subaerial springs Bo3, Bo1, Bo4, Thomas and Anse à la Barque. The Na–HCO_3 waters (springs Bo2, La Lise and Bain du Curé) show much lower TDS values (180–320 mg/kg) and temperatures between 35 and 47 °C.

The other three water types are found only around La Soufrière dome. Calcium–SO_4 waters (springs Bains Jaunes, Carbet Echelle, Galion, Matouba thermale, Pas du Roy, and Tarade) are neutral to slightly acidic and have temperatures of 23–59 °C and TDS of 800–1800 mg/kg. These physical and chemical characteristics suggest that the waters originate through: (a) absorption of H_2S-bearing hydrothermal vapors into shallow, O_2-rich groundwaters; (b) O_2-driven oxidation of H_2S to H_2SO_4; and (c) neutralization of H_2SO_4 through water–rock interaction (Cormy et al. 1970; Demians D'Archimbaud and Surcin 1972, 1976). Calcium–SO_4 springs are the closest to La Soufrière dome (<1.2 km from the summit) and are at comparatively high elevations (950–1170 m a.s.l.). Two thermal springs ~ 3.8 km west of La Soufrière dome (Habitation Revel) at 585 m a.s.l., and Dolé ~ 5.8 km south of the dome at 220 m a.s.l., have a Ca–Na–HCO_3 composition, which makes them very similar to cold springs. They are probably shallow groundwaters heated through conductive heat transfer from below. Two thermal springs ~ 2.5 and 2 km east of La Soufrière dome (Grosse Corde, Carbet) at altitudes of 585–605 m a.s.l. have Ca–Na–Cl compositions. These two waters may originate through mixing of Na–Cl and Ca–SO_4 waters, indicating that the former are not restricted to

Table 1 Chemical composition of waters (concentrations in mg/l). *n.d.* not detected; *n.a.* not analysed

Sample	Code	T (°C)	$\delta^{18}O$ (‰)	δD (‰)	pH	Na	K	Mg	Ca	HCO_3	Cl	SO_4	NO_3	SiO_2	Li	B	Sr	Mn
Cold springs																		
Le Balisier	1	19.2	−2.69	−5.3	7.09	3.8	0.32	0.69	2.98	10	5.2	4.50	0.18	16	n.d.	n.d.	0.009	n.d.
Beaugendre	2	23.5	−2.82	−7.5	6.59	16.2	1.50	4.41	12.9	62	22.3	4.48	7.10	63	n.d.	0.028	0.059	0.0013
Bélair	3	25.6	−2.57	−9.4	6.50	13.0	1.60	7.28	17.3	61	22.5	2.59	21.5	71	n.d.	0.009	0.071	n.d.
Contrebandiers	4	21.8	−2.65	−4.6	6.90	8.4	0.61	2.85	6.51	36	12.9	3.12	0.37	32	n.d.	0.016	0.035	n.d.
Davidon	5	26.3	−2.31	−9.4	6.47	32.1	3.00	5.17	8.14	66	38.1	9.37	0.52	64	0.003	0.033	0.047	0.0014
Dos d'Ane	6	24.3	−2.36	−8.2	6.61	27.4	2.94	10.8	28.6	111	37.8	26.3	17.5	66	0.002	0.097	0.102	0.0014
Duprat	7	24.0	−2.40	−11.2	6.64	17.4	1.10	6.70	15.4	71	28.1	9.02	2.90	83	n.d.	0.031	0.054	n.d.
Etang	8	23.6	−2.59	−5.6	6.91	15.0	2.38	8.78	23.6	89	24.5	7.53	16.8	65	n.d.	0.023	0.075	n.d.
Le Faubourg	9	26.0	−2.64	−9.1	6.39	17.9	3.32	9.20	25.5	109	27.4	12.9	12.4	77	n.d.	0.043	0.097	n.d.
Fonds Cacao	10	26.7	−2.34	−6.9	6.73	22.5	5.16	12.9	39.5	95	44.7	15.3	67.3	83	n.d.	0.039	0.085	n.d.
Grand Camp	11	21.8	−2.33	−9.8	7.23	10.2	2.94	5.18	15.6	61	14.9	12.6	0.25	57	n.d.	0.019	0.044	0.0390
Joséphine	12	22.7	−3.25	−12.1	5.63	8.9	0.80	2.38	9.88	21	18.3	10.8	7.22	54	n.d.	n.d.	0.046	0.0017
La Plaine	13	22.9	−2.64	−8.9	7.75	9.5	2.53	2.43	12.2	44	16.0	3.16	9.22	49	n.d.	0.019	0.035	n.d.
La Source	14	25.9	−2.67	−9.1	6.74	25.7	2.10	9.07	14.0	87	39.0	9.87	7.39	48	n.d.	0.052	0.062	n.d.
Lahaut Fontaine	15	25.4	−2.50	−9.6	6.56	17.9	2.05	4.15	4.35	30	25.3	3.80	5.92	40	n.d.	0.036	0.029	0.0016
Mahaut	16	25.8	−2.67	−7.8	6.63	21.0	1.61	9.81	17.5	119	28.1	3.36	0.44	68	n.d.	0.035	0.071	n.d.
Maison Café	17	23.0	−2.17	−1.4	6.53	14.2	0.78	5.43	15.2	69	17.4	13.2	0.73	50	n.d.	0.020	0.056	n.d.
Matouba froid	18	21.1	−2.75	−9.1	6.03	5.2	0.62	1.79	5.34	25	6.1	4.80	0	29	n.d.	n.d.	0.019	n.d.
Morne Rouge	19	25.8	−3.02	−7.9	5.81	10.4	0.50	1.88	4.34	23	15.8	1.97	1.83	33	n.d.	0.014	0.021	0.0038
Pare Archéologique	20	24.7	−2.53	−4.4	6.66	15.7	3.09	12.1	35.1	127	29.2	15.1	19.2	70	n.d.	0.033	0.125	n.d.
Petite Fontaine	21	23.7	−2.82	−9.8	8.15	61.9	1.17	29.4	31.4	210	103	11.6	5.69	63	n.d.	0.098	0.148	n.d.
Sofaia cold	22	24.3	−2.67	−8.3	5.34	8.9	0.57	2.07	2.44	16	15.4	2.69	0.30	24	n.d.	n.d.	0.014	0.0047
Tabaco	23	22.7	−2.88	−7.2	6.74	7.9	2.61	2.39	10.2	36	12.9	3.20	6.91	50	n.d.	0.018	0.027	n.d.
Thermal springs																		
Thomas	Th	41.0	−0.02	4.0	7.45	8580	296	1110	496	128	15300	2280	n.d.	81	0.541	5.02	6.50	0.125
Anse à la Barque	AB	34.4	−2.42	−5.3	7.43	807	25.4	120	102	205	1410	218	n.d.	103	0.029	0.395	1.07	n.d.
Bouillante 1	Bol	46.8	−2.45	−6.2	7.03	128.8	11.9	6.50	46.3	176	190	17.4	1.19	92	0.049	0.231	0.242	n.d.
Bouillante 3	Bo3	74.2	−0.75	−0.9	6.63	5800	572	18.8	2270	140	12800	154	n.d.	220	5.14	13.0	17.9	2.77
Bouillante 4	Bo4	68.8	−3.15	−11.5	6.17	305.4	28.4	4.84	90.8	149	524	97.1	4.31	135	0.151	0.429	0.740	0.547
Bouillante 2	Bo2	46.9	−2.88	−9.3	7.58	75.1	9.01	5.25	26.4	194	61.5	9.84	3.48	110	0.012	0.112	0.096	n.d.
Bain du Curé	BC	49.6	−2.84	−6.5	7.60	45.9	6.89	2.93	22.8	143	27.1	6.43	0.87	80	0.010	0.042	0.075	n.d.
La Lise	L	44.9	−2.75	−5.6	7.33	41.9	3.89	4.84	13.4	132	27.5	5.69	1.14	72	0.004	0.047	0.055	0.0110
Matouba thermale	M	58.8	−2.69	−7.1	5.65	33.8	8.19	12.0	257	23	18.1	708	0.22	37	n.d.	0.068	0.515	0.698
Pas du Roy	PR	40.1	−2.56	−7.9	5.59	59.4	8.72	49.8	169	64	85.9	580	0.16	115	0.009	0.441	0.111	2.06
Tarade	Ta	44.4	−2.67	−3.5	6.07	75.0	14.1	58.2	194	104	142	579	0.17	111	0.008	0.592	0.122	0.0030
Bains Jaunes	BJ	27.7	−2.77	−5.9	5.02	40.6	4.96	27.3	101	18	46.8	384	0.15	102	0.011	0.264	0.094	1.63
Carbet Echelle	CE	22.7	−2.69	−5.6	5.50	38.5	7.04	66.3	225	120	17.5	876	0.14	100	0.009	0.097	0.156	6.56
Galion	G	43.4	−2.44	−5.9	4.84	74.4	20.5	75.4	229	35	167	875	0.44	165	0.007	0.918	0.052	5.47
Chute du Carbet	CC	44.9	−2.05	−4.9	6.51	116.2	24.0	64.9	188	125	368	303	0.20	110	0.014	0.317	0.477	n.d.
Grosse Corde	GC	48.6	−2.20	−5.0	6.37	128.7	23.6	70.9	180	103	557	180	0.36	110	0,008	0.719	0.661	n.d.
Dolé	D	40.6	−2.41	−5.4	6.52	28.6	5.68	16.7	40.0	148	34.2	60.7	4.81	62	0.004	0.062	0.116	n.d.
Habitation Revel	HR	42.7	−2.98	−6.8	6.45	22.4	3.29	4.78	18.8	112	9.6	15.0	2.90	61	0.017	0.026	0.058	n.d.
HS 2[a]	HS2	92.0	0.13	3.9	6.05	8069	587	1014	1014	162	17053	1662	0	131	0.83	7.57	n.a.	n.a.
HS 1[a]	HSI	55.0	0.43	5.8	n.a.	n.a.	n.a.	n.a.	n.a.	n.a.	n.a.	n.a.	n.a.	n.a.	n.a.	n.a.	n.a.	n.a.
SW		26.8	1.11	10.5	n.a.	n.a.	n.a.	n.a.	n.a.	140	18055	2646	n.a.	n.a.	n.a.	n.a.	n.a.	n.a.
SW[a]		28.7	0.52	7.3	8.20	10575	446	1434	445	134	19854	2786	0	0.18	0.139	4.97	n.a.	n.a.
wells																		
B2[a]	B2		−1.51	−1.7	n.a.	4897	758	0.97	1812	15.3	11664	13.5	0	457	2.98	10.9	n.a.	n.a.
B4[a]	B4		n.a.	n.a.	n.a.	4391	547	0.97	1804		10636	28.8	0	284	2.64	11.0	n.a.	n.a.

[a] Analyses taken from Traineau et al. (1997)

Table 2 Stable water isotopic composition and gas composition (μmol/mol of total discharge) of fumaroles

Sample	T (°C)	$\delta^{18}O$ (‰)	δD (‰)	H_2O	CO_2	H_2S	H_2	$N_2 (+O_2)$	CH_4	CO
S1	95.0	−8.86	−34.5	974260	23110	1220	1223	188	0.113	0.014
S2	93.5	−1.98	−24.0	970710	25340	2152	1525	271	n.d.	0.114
S3	94.0	−2.51	−25.9	959000	23690	50	157	16870	n.d.	0.198
S4	94.5	−10.35	−45.0	962330	34050	1841	1427	348	2.31	0.033
S5	94.5	−10.60	−42.8	933770	59960	3424	2275	566	2.84	0.029
B	92.1	−7.60	−35.7							

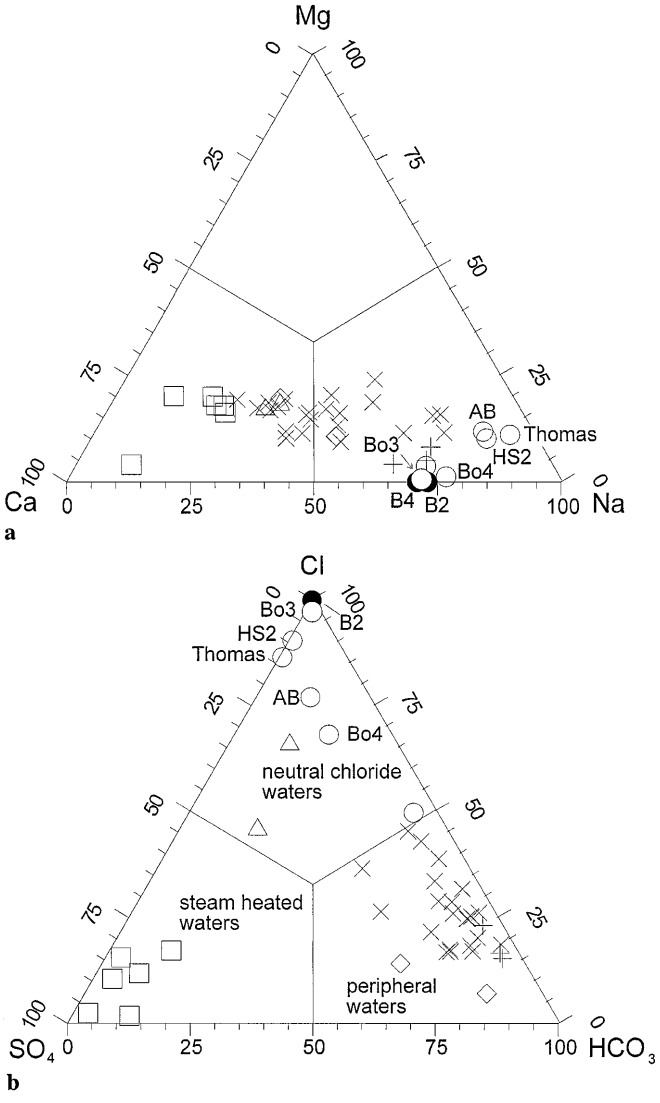

Fig. 3 **a** Ca–Mg–Na; **b** SO_4–HCO_3–Cl triangular diagrams (from Giggenbach 1988). For symbols see Fig. 1. B2 and B4 (*filled circles*) refer to the geothermal waters sampled in the wells B2 and B4 (Traineau et al. 1997)

the Bouillante area but are also present underneath La Soufrière.

This chemical zoning of the groundwaters circulating in La Soufrière area suggests the presence of a central steam-dominated zone and an external zone, where the shallow groundwaters are affected either by input of heat from below or addition of Na–Cl liquids coming from geothermal aquifer(s).

The cold springs have variable compositions, from Ca–HCO_3 to Na–HCO_3-Cl, and TDS of 36–360 mg/kg. Their outlet temperatures (19.2–26.7 °C) are very close to the average annual air temperature, suggesting that these waters circulate in shallow aquifers.

Chloride diagrams

Correlation plots between B, Cl, and the $^{18}O/^{16}O$ ratio have been prepared to look for possible mixing and/or boiling processes that could explain the origin of thermal springs (Fig. 4a,b). The Cl-rich waters, samples Bo3, HS2, Thomas spring, and Anse à la Barque, are considered first.

The composition of the spring Bo3 corresponds to that of a boiled geothermal liquid in Fig. 4a. Dilution by local groundwater also occurs, as indicated by Fig. 4b. Steam separation and dilution, the two main processes affecting thermal waters during their rise to the surface, are nearly independent and may take place in any order (Giggenbach and Stewart 1982). Therefore, the chemical and isotopic compositions of sample Bo3 can be attained either through steam loss of an already diluted, cooled geothermal water, or through steam loss of the original geothermal liquid and subsequent dilution. The fraction of diluting cold waters can be estimated to be close to 0.2, as shown by the solid line in the $\delta^{18}O$ vs Cl diagram.

The origin of the Thomas spring cannot be attributed to steam heating of a binary seawater–groundwater mixture. In that case the Thomas sample should be on the line connecting these two end members in Fig. 4a, since input of steam would simply move the point toward the origin of the axes without shifting it from this mixing line. Conductive heating of a binary seawater–groundwater mixture can also be ruled out, since the Thomas sample should be on the dilution line of local seawater in Fig. 4a. The point representing Thomas spring lies above the dilution line of local seawater, toward the geothermal liquid; thus we conclude that this spring discharges a mixture made of seawater, local groundwater, and geothermal water (either boiled or not), in order of decreasing importance. The same conclusion was also reached by Traineau et al. (1997).

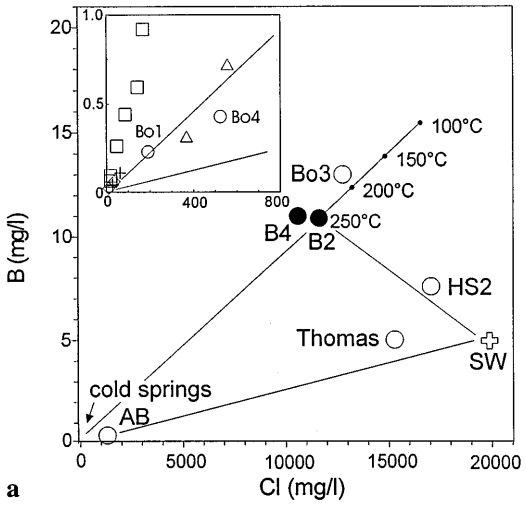

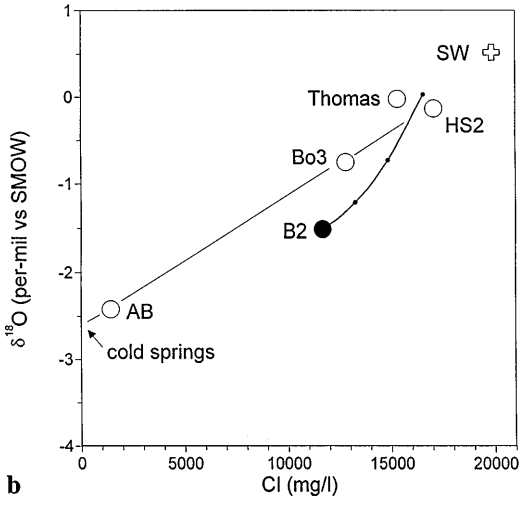

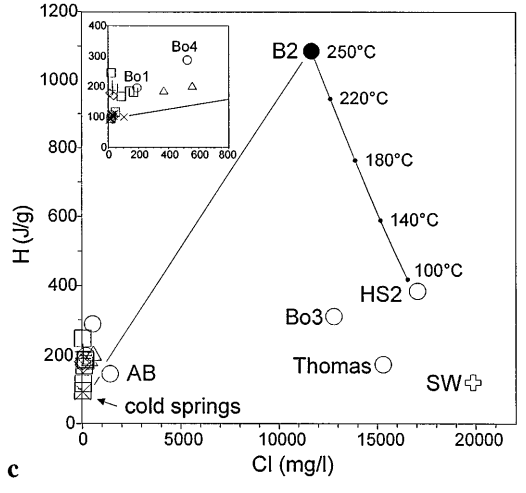

Fig. 4 Plots of chloride vs **a** boron, **b** $\delta^{18}O$, and **c** enthalpy. For symbols see Fig. 1. B2 and B4 (*filled circles*) refer to the geothermal waters sampled in the wells B2 and B4 (Traineau et al. 1997). *SW* refers to local seawater. The single-step vapor separation curve was calculated starting from liquid B2 at 250 °C

The thermal spring Anse à la Barque, which is on the dilution line of local seawater (Fig. 4a), is instead a binary seawater–groundwater mixture heated through either steam input or conductive heat transfer.

Spring HS2 could originate through mixing of the unboiled, undiluted geothermal water with local seawater. However, the involvement of boiled instead of the original geothermal water, coupled with dilution by local groundwater, cannot be ruled out, on the basis of Fig. 4a,b, but it seems unlikely from the enthalpy–chloride plot (Fig. 4c; Fournier 1979a).

Figure 4c permits evaluation of whether fluids are heated conductively or by steam. In both cases heat is brought to the water without increasing its Cl content in contrast to the admixture of geothermal water in which heat and Cl content increase proportionally to the amount of geothermal liquid added. All the remaining thermal springs, except the samples Bo3, Thomas spring, Anse à la Barque, and HS2, show higher enthalpy than that obtained by admixure of geothermal water to cold groundwater; therefore, they have to be considered as steam-heated or conductively heated waters. For the two Na–Cl fluid samples Bo4, Bo1 (Bouillante region), and the Ca–Na–Cl waters (Soufrière), an input of geothermal liquid is needed to explain their relatively higher Cl concentrations, as confirmed by the B vs Cl plot (low content region; inset in Fig. 4a) and, for the Ca–Na–Cl springs, by isotopic data as well (see below).

The main constituents of the steam separated from a deep geothermal liquid are, besides water vapor, CO_2 and H_2S. When this steam condenses into upper-level, O_2-rich aquifers, the reduced sulphur species (mainly H_2S) are oxidized to sulphuric acid, and the absorption of CO_2 results in the formation of carbonic acid. The production of either H_2SO_4 or H_2CO_3 obviously tends to reduce the pH of the fluid, at least before the acids are neutralized through water–rock interaction. This process changes the SO_4 content as well as the concentration of total inorganic carbon (TIC), i.e., $CO_{2,aq} + HCO_3 + CO_3 +$ related aqueous complexes. Therefore, steam-heated waters can be tentatively distinguished from conductively heated waters by higher SO_4 and TIC contents and lower pH values, as is the case for the Ca–SO_4 thermal waters (Fig. 5; Table 1). Only a slightly higher TIC is noticed for the spring Bo4. Consequently, the Ca–SO_4 waters of La Soufrière and probably spring Bo4 represent steam-heated waters, whereas the remaining thermal waters could be considered as conductively heated. Furthermore, most of the Ca-SO_4 thermal waters exhibit relatively higher B (Fig. 4a) contents, which could be related to input of geothermal steam separated at high temperatures, as B enters in significant amounts into the vapor phase during boiling from a geothermal liquid at temperatures higher than 200 °C, although its vapor-liquid distribution coefficient is less than 1 at any temperature (Ellis and Mahon 1977, and references therein).

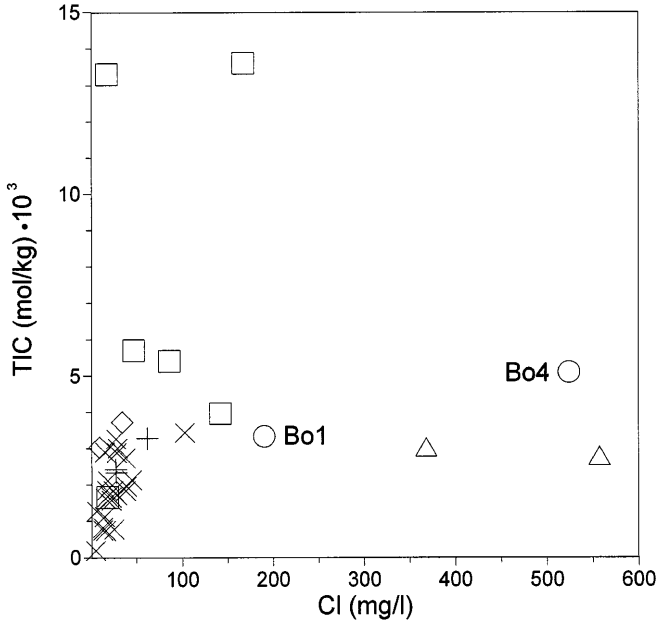

Fig. 5 Plot of total inorganic carbon (*TIC*) vs Cl (mg/l). Symbols as in Fig. 1

Geothermometers

One of the most valuable graphical geothermometric techniques is the ternary plot Na–K–$Mg^{1/2}$ (Fig. 6; Giggenbach 1988). It provides simultaneous comparison of the temperature dependence of the concentration quotients Na/K and K^2/Mg, which are controlled, in fully equilibrated geothermal liquids, by mineral-solution equilibria involving albite, K-feldspar, illite, chlorite, and a silica mineral (either chalcedony or quartz). The samples of geothermal wells B4 and B2 plot along the full equilibrium line, suggesting that their cation ratios are controlled by mineral-solution equilibrium. Corresponding Na–K- and K–Mg-temperatures are 270 and 263 °C for well B2 and 250 and 245 °C for well B4. The reservoir temperatures calculated by means of the quartz geothermometer (Fournier and Potter 1982) and the Na–K geothermometer (Fournier 1979b) are 244 and 258 °C for well B2 and 205 and 237 °C for well B4. Most of these values are either close to or slightly higher than the maximum temperature measured in the geothermal wells (245 °C; Traineau et al. 1997). This suggests that the geothermal liquid experienced some cooling before entering the well. The geothermometers did not have enough time to reequilibrate at these lower temperatures and thus still have a memory of the higher temperature values, which are presumably present in the geothermal reservoir at some distance from the well. The comparatively low quartz temperature of well Bo4, 205 °C, indicates the likely precipitation of amorphous silica prior to analysis, possibly due to improper preservation of the sample.

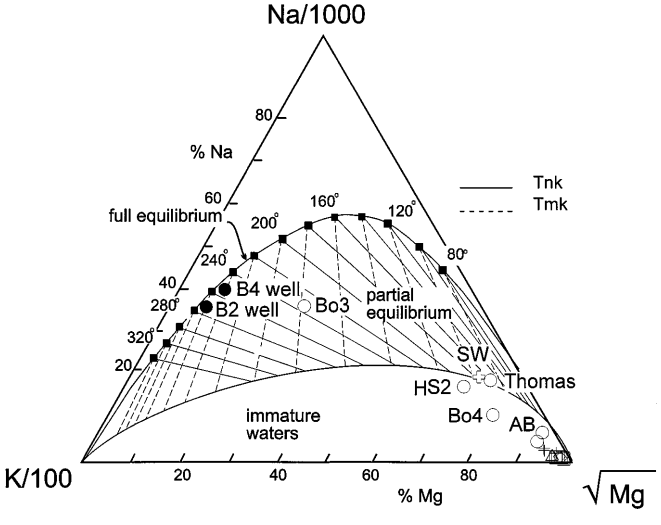

Fig. 6 Na–K–$Mg^{1/2}$ triangular plot (modified from Giggenbach 1988). For symbols see Fig. 1

As shown above, the spring receiving the largest contribution of geothermal liquid is Bo3. It plots in the field of partially equilibrated geothermal liquids in Fig. 6, and its apparent equilibrium temperatures are as follows:

T_{Na-K} = 231 °C, using the Na–K geothermometer of Giggenbach (1988)
T_{Na-K} = 216 °C, using the Na–K geothermometer of Fournier (1979b)
T_{K-Mg} = 179 °C, using the K–Mg geothermometer of Giggenbach (1988)
T_{quartz} = 187 °C, using the quartz geothermometer of Fournier and Potter (1982)

The relatively low temperatures provided by the K–Mg and quartz geothermometers are not surprising, because these geothermometers are strongly affected by dilution. Conversely, Na–K temperatures are comparatively high, as the Na–K geothermometer is only slightly affected by dilution. Moreover, the apparent equilibrium temperatures might also differ because of the different rate of reequilibration of these geothermometers, with the K^2/Mg ratio and the SiO_2 content re-equilibrating faster than the Na/K ratio upon cooling (Giggenbach 1988). However the Na–K temperatures of sample Bo3 are significantly lower than those of wells B2 and B4, indicating that the geothermal liquid takes a comparatively long time to move from the reservoir to the surface, sufficient for some readjustments of the Na/K ratio to decreasing temperatures.

The Cl-rich, Na–Cl thermal waters (Thomas, HS2, Bo4, Anse à la Barque), as well as all the other thermal waters, plot in the area of "immature waters." For these waters the evaluation of equilibrium temperatures is not applicable.

Reaction path modelling

As already recognized by Traineau et al. (1997), the geothermal reservoir of Bouillante is fed by a mixture

of seawater and meteoric water, the contributions of which are close to 60 and 40%, respectively; and strontium isotopes suggest that this mixture evolves to the composition of the Bouillante geothermal liquid through interaction with mainly andesitic host rocks.

To evaluate this interpretation, the concentrations of chemical species in the aqueous solution, and the moles of precipitating minerals during this water–rock interaction process, were computed by means of the software package EQ3–6 (Wolery 1979, 1992; Wolery and Daveler 1992). The initial aqueous solution was considered to be a mixture of 60% local seawater and 40% average rainwater collected in the Western North Atlantic area (Berner and Berner 1996). An average andesite (Wilson 1989) was taken to be representative of the interacting rocks; after recalculating its composition on an elemental basis, it was introduced in the EQ6 input file as a reactant. EQ6 was run in reaction progress mode, without any kinetic constraints. The P_{CO2} was considered to be governed by a CO_2 reservoir at 0.32 bar, which corresponds to the value evaluated for well B2 by using the K–Ca geobarometer by Giggenbach (1988).

Only analcime, anhydrite, 14A-clinochlore, epidote, hematite, kaolinite, muscovite, and quartz were precipitated during the simulation. The final mineral assemblage, after the titration of 2.1 moles of andesite/kg of water, was made of analcime, anhydrite, 14A-clinochlore, epidote, hematite and quartz. All these solid phases are possible hydrothermal alteration minerals in active geothermal systems. The calculated composition of the aqueous solution, in mg/kg, (Na = 5390, K = 682, Mg = 13.3, Ca = 1530; Cl = 11600; SO_4 = 6.8; HCO_3, including CO_2 and CO_3, = 203; SiO_2 = 375), is in satisfactory agreement with that of well B2, confirming that the Bouillante geothermal liquid can be the product of this water–rock interaction process.

The initial and final pH values of the aqueous solution are 6.6 and 5.3, respectively. The final pH is close to the value of 5.4 calculated from temperature, P_{CO_2} and salinity by means of the equation of Chiodini et al. (1991), and is evidently fixed by mineral-solution equilibria. Similar values (5.3–5.5) were also obtained by Reed (1997) through titration, at 300 °C, of andesite with an acidic fluid, i.e., a metal-rich volcanic gas condensate from a high-temperature fumarole on Augustine volcano, diluted 1:10 with meteoric water.

Gas chemistry

Water (934,000–974,000 μmol/mol) is the main constituent of all the sampled fumarolic fluids, followed by CO_2 (23,100–60,000 μmol/mol), H_2S (1220–3420 μmol/mol), and H_2 (1220–2280 μmol/mol). Nitrogen contents are generally lower than 600 μmol/mol, with the exception of sample S3, which is heavily contaminated by air and therefore not further considered. Methane (undetectable to 2.84 μmol/mol) and CO (0.0142–0.114 μmol/mol) are minor constituents (Table 2).

All the fluids have some hydrothermal characteristics, e.g., H_2S is the main S-species, whereas SO_2 and other highly acidic gases (HCl, HF) are virtually absent (e.g., Giggenbach et al. 1990). In most hydrothermal systems, CH_4 contents are much greater than CO concentrations (Chiodini and Marini 1998). However, this is not true for the fumaroles at the summit of La Soufrière dome, and their undetectable CH_4 indicates relatively oxidizing conditions that could point to the involvement of magmatic fluids.

Gas geothermometry

Thermodynamic conditions at depth can be evaluated assuming that chemical equilibrium among gas species is attained in the hydrothermal environment and is quenched during the upflow of the hydrothermal fluids. Expected compositions of gaseous mixtures can be computed using different theoretical models, which assume either attainment of internal equilibrium among gaseous H_2O, H_2, CO_2, CO, and CH_4 or equilibration of these gas constituents with unspecified minerals acting as f_{O2} buffers. Both models have been recently reviewed by Chiodini and Marini (1998).

The first model is illustrated by means of a gas ratio diagram (Fig. 7), where $L_1 = \log (X_{H_2O}/X_{H_2}) + \log$

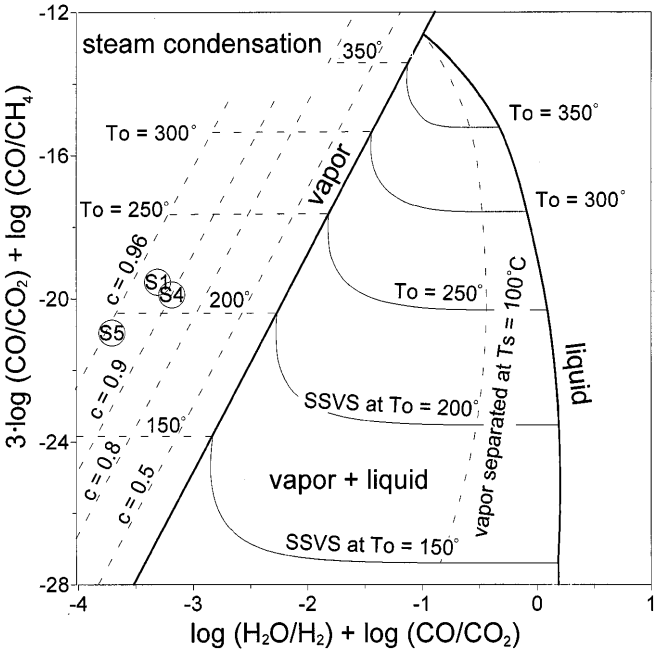

Fig. 7 Plot of 3 log (CO/CO_2) + log (CO/CH_4) vs log (H_2O/H_2) + log (CO/CO_2). The *SSVS* curves refer to the vapor phases produced by boiling of a single liquid phase (initial temperature *To*) and separated in a single step at temperature *Ts*. The compositions of equilibrated, single vapor phases affected by steam condensation at Tc = 100 °C (*dashed lines*) are also shown. *c* fraction of condensed steam. *Circles* fumarolic fluids. Codes are given in Table 2

(X_{CO}/X_{CO_2}) and $L_2 = 3 \log (X_{CO}/X_{CO_2}) + \log (X_{CO}/X_{CH_4})$ are represented on the axes. The theoretical values for these sums of log ratios in a single saturated vapor phase and in a single saturated liquid phase are shown as vapor lines and liquid lines, respectively. It is generally accepted that fumaroles discharge vapors produced through boiling of a single liquid phase. Therefore, the composition of vapors generated through single-step vapor separation at temperature Ts, from boiling liquids the original temperatures of which are To, are also reported (single-step vapor separation, SSVS lines). Furthermore, a steam-condensation grid is also shown. The latter is obtained assuming: (a) either attainment of equilibrium in a single saturated vapor phase or attainment of equilibrium in a single saturated liquid phase and subsequent occurrence of steam separation at Ts very close to To; and (b) final occurrence of steam condensation through conductive heat loss at Tc = 100 °C. All the fumarolic samples from La Soufrière plot above the vapor line, indicating the occurrence of steam condensation, in agreement with their comparatively low discharge temperature (near the boiling point of water) and flow rates. Equilibrium temperatures are between 191 and 215 °C, and the fractions of condensed steam range from 0.900 to 0.955. As the CH_4 content of sample S2 is below detection, using the known L_1 value of –2.54 and estimating the equilibrium temperature at 260 °C. (This value is obtained by adding 40 °C to the equilibrium temperature indicated by the log (X_{H_2}/X_{H_2O}) vs log (X_{CO}/X_{CO_2}) plot of Fig. 8), the calculated steam fraction amounts to 0.845.

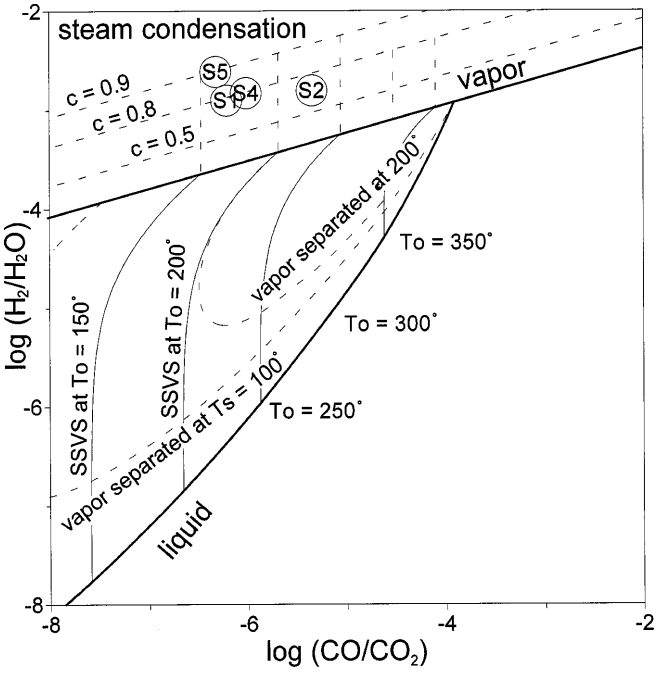

Fig. 8 Plot of log (H_2/H_2O) vs log (CO/CO_2). The theoretical grid assumes that redox conditions in the gas equilibration zone are controlled by the f_{O_2}-buffer of D'Amore and Panichi (1980). Theoretical lines and symbols as in Fig. 7

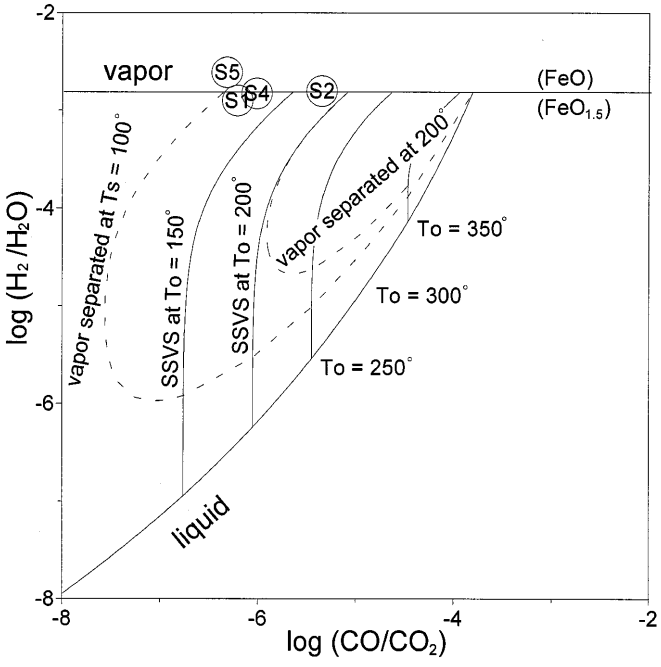

Fig. 9 Plot of log (H_2/H_2O) vs log (CO/CO_2). The theoretical grid assumes that redox conditions in the gas equilibration zone are controlled by the FeO–$FeO_{1.5}$ hydrothermal buffer of Giggenbach (1987). Theoretical lines and symbols as in Fig. 7

In the second model the theoretical compositions are obtained from either of two commonly used redox buffers, (a) the (FeO)–($FeO_{1.5}$) buffer of Giggenbach (1987), where f_{O_2} is linked to temperature through

$$\log f_{O_2} = 10.736 - 25414/T, \quad (1)$$

and (b) the empirical relationship of D'Amore and Panichi (1980):

$$\log f_{O_2} = 8.20 - 23643/T. \quad (2)$$

Also in Figs. 8 and 9, the theoretical values of log (X_{H_2}/X_{H_2O}) and log (X_{CO}/X_{CO_2}) are shown as vapor, liquid, SSVS, and steam condensation lines. The spread of samples in Fig. 8 (where the theoretical grid is based on the redox buffer of D'Amore and Panichi 1980) is similar to that in the L_1–L_2 plot (Fig. 7), although the calculated equilibrium temperatures are 30–50 °C lower than those computed for the L_1–L_2 plot and the fractions of condensed steam range from 0.7 to 0.895.

Considering the rock buffer of Giggenbach (Fig. 9), all the samples plot relatively close to the equilibrium vapor line. In this case no occurrence of steam condensation is shown.

Isotope geochemistry

δD and δ^{18}O values

The δD vs δ^{18}O diagram (Fig. 10) shows the worldwide meteoric water line ($\delta D = 8 \times \delta^{18}O + 10$) and the local meteoric water line ($\delta D = 8 \times \delta^{18}O + 16$), which is based

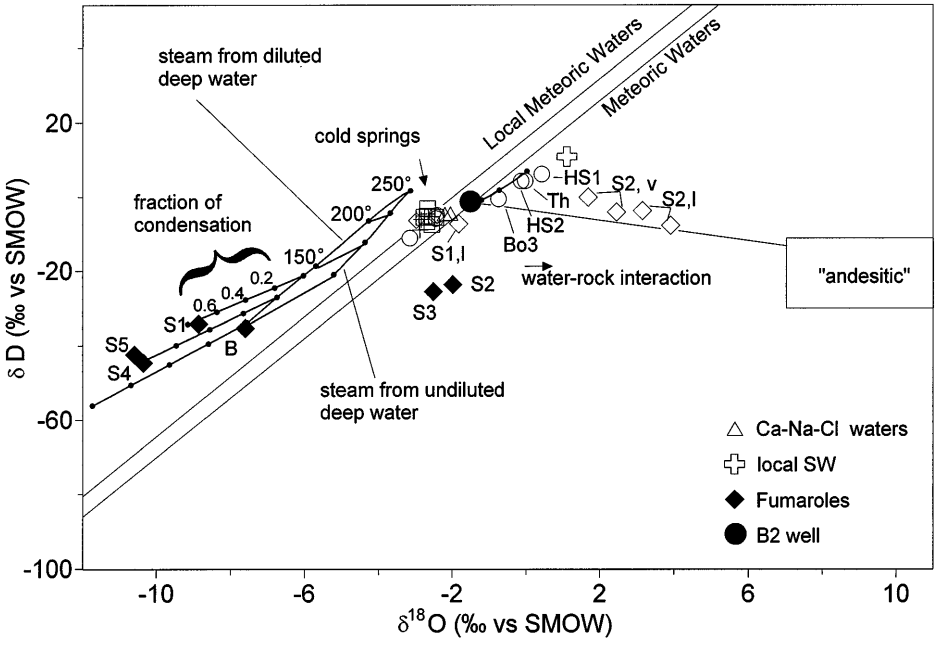

Fig. 10 δD vs δ^{18}O diagram, showing the isotopic composition of waters and vapors discharging at Basse Terre. Also shown are the worldwide and local meteoric water lines, the composition of arc-type magmatic waters (Giggenbach 1992a), the isotopic composition of steam and water formed through boiling of the B2 geothermal liquid either undiluted or after dilution with local groundwater, and a steam condensation grid for a condensation temperature of 100 °C

on rain waters sampled on Basse-Terre at different elevations (Benauges 1981).

Also shown are the isotopic compositions of the steam and water produced through boiling of the geothermal liquid (sample B2), either pure or diluted, assuming single-step steam separation and an initial temperature of 250 °C. This value is close to the equilibrium temperatures obtained by different geothermometers and to the maximum temperatures measured in deep geothermal wells. The effects of dilution on the geothermal liquid were taken into account by assuming a temperature of 25 °C, a δD value of –9‰, and a δ^{18}O value of –2.7‰ for the diluting groundwater. Calculations were carried out following the interpretative framework of Giggenbach and Stewart (1982).

A steam condensation grid is also reported in Fig. 10. The condensation lines were calculated, assuming that steam condensation takes place through conductive heat losses at a constant temperature of 100 °C, through the expression:

$$\delta_{S,C} = \delta_{S,O} - 1000 \times \ln \alpha \times c. \quad (3)$$

Equation (3) is based on the isotope balance (single-stage separation is assumed):

$$\delta_{S,O} = \delta_{S,C}(1-c) + \delta_{L,C} \times c \quad (4)$$

and on the hypothesis of liquid-vapor isotope equilibrium:

$$\delta_{L,C} = \delta_{S,C} = 1000 \times \ln \alpha, \quad (5)$$

where subscripts S,O; S,C; and L,C refer to the steam before condensation, the steam remaining after condensation, and the condensate, respectively, whereas c is the fraction of condensed steam. The liquid–vapor equilibrium fractionation factors $1000 \times \ln\alpha$ at 100 °C is 5.24 for ^{18}O and 27.8 for D (Truesdell et al. 1977). The compositional range for magmatic andesitic waters (Giggenbach 1992a) is also shown in Fig. 10.

Cold groundwaters generally plot between the line of local meteoric waters and the worldwide meteoric water line. The Na–HCO_3, Ca–SO_4, and Ca–Na–HCO_3 thermal waters, as well as some Na–Cl thermal waters, are situated in the same field of cold waters. This indicates that they have a similar origin, predominantly meteoric. The remaining Na–Cl waters (Bo3, HS1, HS2, Thomas) are heavier than the geothermal liquid B2, due to mixing with local seawater and/or boiling. As this mixing line is very close to the boiling line, Fig. 10 is not the best plot to identify these processes. The Ca–Na–Cl waters are on the mixing line of the geothermal liquid B2 with local groundwater, in agreement with chemical evidence.

The geothermal liquid B2 plots on the worldwide meteoric water line and is shifted by only ~0.7 ‰ from the local meteoric water line. The liquid lies on the mixing trend between local groundwaters and seawater and seems to be produced by simple mixing of these two end members (as already recognized by Traineau et al. 1997) with no detectable contribution of magmatic andesitic water and with no appreciable ^{18}O shift attributable to water–rock isotope exchange. If so, the Bouillante geothermal reservoir can be considered a dynamic, water-dominated system, according to Giggenbach (1992b).

The fumarolic fluids exhibit a large spread in δD and δ^{18}O values. The fumarolic sample from the Bouillante steaming grounds (B) is a vapor either separated from the geothermal liquid B2 after dilution with cold groundwater down to 100 °C, or produced through steam separation at ~100 °C from the undiluted geothermal liquid followed by condensation or by an intermediate process.

The fumarolic fluids collected in the Ty fault area (S1, S4, S5) show isotopic compositions even lighter than that of sample B, which can only be explained by the occurrence of steam condensation, in agreement with the indications of gas chemistry. Comparison of the analytical data with the theoretical vapors generated through boiling of either undiluted or diluted geothermal liquid B2 indicates that samples S1, S4, and S5 could be produced through steam separation either at 120–140 °C from the pre-diluted geothermal liquid B2 or at 100–120 °C from the undiluted geothermal liquid B2; however, these separation temperatures are much lower than those indicated by gas chemistry (191–215 °C). A different interpretation is possible taking into account the findings of gas chemistry, i.e., the fractions of condensed steam and the temperatures of steam separation. Starting from the analytical δD and δ^{18}O values, the isotopic compositions of the vapor phases before condensation were calculated by means of Eq. (3). Then the isotopic compositions of the corresponding liquid phases at separation temperatures were computed, assuming liquid–vapor isotope equilibrium. The liquid phase presumably involved in the genesis of sample S1 (S1,l) has calculated δD and δ^{18}O values (–7.7 and –1.83‰, respectively) that are similar to those of geothermal liquid B2, considering the uncertainties of this reconstruction and the complexities of natural processes.

The two fumarolic samples from the top of La Soufrière dome (S2 and S3) fall to the right of the meteoric water lines, suggesting the involvement of magmatic andesitic waters. Steam condensation evidently affected these samples, as shown by the gas composition data of sample S2. Assuming steam condensation through conductive heat loss at 100 °C and a fraction of condensed steam of 0.7–0.845 for sample S2 (as indicated by gas chemistry), the δD and δ^{18}O values of the vapor phase before condensation (S2,v), obtained through Eq. (3), are –0.5 to –4.5 ‰ and +1.69 to +2.45‰, respectively. Both this vapor and the hypothetical liquid from which it was possibly separated at 260 °C (S2,l with δD = –4.1 to –8.1‰ and δ^{18}O = +3.15 to +3.91‰) plot on the mixing trend between the geothermal liquid B2 and andesitic magmatic waters, confirming that the vents on top of La Soufrière dome are fed by a peculiar zone of the underlying hydrothermal aquifer, which receives considerable input of magmatic fluids from below. However, the ^{18}O shift of these samples could also be due to water–rock interaction processes. This possibility cannot be ruled out, as the δD value of the local meteoric waters is close to that of the "andesitic waters," typically the case for groundwaters prevailing over tropical to temperate climates (Giggenbach 1997).

Steam separation at comparatively high temperature in the Soufrière area is also suggested by the high B contents of the Ca–SO_4 thermal waters discharging around the dome, which are considered to be heated through steam input. In principle, steam-heated waters should be shifted toward the composition of the steam in the δD vs δ^{18}O diagram. Since this shift is not evident for the Ca–SO_4 thermal waters, the steam heating these waters must have an isotopic composition close to that of local groundwaters. Such a steam might be produced through separation at high temperature from a geothermal liquid isotopically very similar to that produced from the geothermal well B2.

Conclusion

The Soufrière is a high-risk volcano, since a population of approximately 70,000, including the capital Basse-Terre of Guadeloupe, is within a few kilometers of the volcano. The delineation of the conceptual geochemical model of La Soufrière-Bouillante system represents a necessary basis for adequate volcanic surveillance as well as for further geothermal exploration.

The high-salinity Na–Cl liquid circulating in the comparatively deep geothermal reservoir of Bouillante is a mixture of seawater and meteoric water, as indicated by conservative chemical constituents (e.g., Cl and Br) and δD and δ^{18}O values of water (Traineau et al. 1997). This diluted seawater becomes depleted in Mg, SO_4, Na, and enriched in Si, K, and Ca through interaction with host rocks, mainly andesite, at temperatures close to 250 °C and also obtains a $^{87}Sr/^{86}Sr$ ratio similar to that of andesite (Traineau et al. 1997). Reaction-path modelling indicates that an aqueous solution very similar to the Bouillante geothermal liquid B2 is produced through titration of 2.1 mol of andesite/kg of water, accompanied by precipitation of analcime, anhydrite, 14A-clinochlore, epidote, hematite, kaolinite, muscovite and quartz, at a temperature of 250 °C and P_{CO_2} of 0.32 bar. Contrary to what is observed in many other high-temperature geothermal systems, the Bouillante geothermal liquid shows no appreciable oxygen shift. This excludes both the addition of ^{18}O-rich andesitic, magmatic waters, and appreciable water–rock oxygen-isotope exchange, suggesting that the Bouillante geothermal liquid has a relatively short residence time in the geothermal reservoir. The reservoir can be considered a dynamic, water-dominated system according to Giggenbach (1992b). One important practical implication is the low probability of encountering acid fluids in the deep wells of the Bouillante geothermal reservoir.

In the Bouillante area, the Na–Cl liquid of the Bouillante geothermal reservoir ascends toward the surface and experiences a combination, in different proportions, of boiling and mixing with groundwater or seawater, finally discharging at springs Bo3, HS2, Thomas and, although in subordinate amounts, Bo4 and Bo1 as well. These springs define a zone of major upflow of the Na–Cl geothermal liquid, which is contoured by the Na–HCO_3 thermal springs Bo2, Bain du Curé and La Lise, and by the Na–Cl thermal spring of Anse à la Barque, all conductively heated. Although some weak steaming ground is present in a small part

of the Bouillante area, the absence of steam-heating phenomena agrees with the comparatively low outlet temperatures of thermal springs, peaking at 74 °C for subaerial features (Bo3) and 92 °C for subaqueous features (HS2).

Two main fumarolic fields are present in La Soufrière area; one is at the top of the dome and includes a high-flow-rate central vent, and the second is at the southeastern foot of the dome, in the Ty fault area. These fumarolic vapors likely form through boiling of typical hydrothermal aqueous solutions, as suggested by the absence of highly acid gases, e.g., HCl, HF, and SO_2 (e.g., Giggenbach et al. 1990). However, the fumarolic vapors of the dome summit have undetectable CH_4, which could be ascribed to the input of relatively oxidizing magmatic fluids into the zone of the hydrothermal aquifer connected with this site. Other convincing evidence is provided by the δD and δ^{18}O values of the fumarolic fluids discharged by the vents of the dome summit, which may indicate addition of magmatic fluids.

Considering equilibration of H_2O, H_2, CO_2, CO, and CH_4 with unspecified minerals acting as f_{O2} buffers (D'Amore and Panichi 1980), the obtained equilibrium temperatures range from 160 to 180 °C for the fumaroles of the Ty fault area and reach almost 230 °C for vent S2, near the dome summit. Alternatively, assuming attainment of internal equilibrium among these gas constituents, computed equilibrium temperatures are between 190 and 215 °C for the fumaroles of the "Ty" fault area. The absence of detectable CH_4 in the summit vents prevents application of this approach. Nevertheless, systematic, nearly constant differences are observed between the temperatures calculated with the two techniques, so that an equilibrium temperature close to 260 °C can be reasonably hypothesized for the summit fumarolic vents. In summary, the temperatures of the boiling hydrothermal aquifer beneath La Soufrière dome are 190–215 °C below the Ty fault area and close to 260 °C below the dome summit. This higher temperature is caused by input of hot magmatic fluids in the zones of the aquifer below the dome summit.

Gas geothermometric techniques also indicate that steam condensation is an important phenomenon affecting all the fumarolic vents, with the fractions of condensed steam reaching values of 0.85–0.95. Therefore, the δD and δ^{18}O values of fumarolic fluids have been corrected for the effects of steam condensation, on the basis of gas chemistry and assuming that the temperatures of liquid–vapor separation are nearly equal to equilibrium temperatures. The boiling liquid phase producing the fumarolic fluids of the Ty fault area has calculated δD and δ^{18}O values similar to those of the Na–Cl liquid of the Bouillante geothermal reservoir. Applying the same corrections to the fumarolic fluid coming from the top of La Soufrière dome, the liquid from which it is separated at 260 °C must be strongly enriched in ^{18}O. This ^{18}O shift can be ascribed to either oxygen isotope exchange with rocks or mixing of a geothermal liquid similar to that of the Bouillante geothermal reservoir with andesitic magmatic waters. The oxidizing character of the summit fumaroles and the absence of detectable ^{18}O shift for the geothermal liquid of the Ty fault fumaroles favor mixing. In addition, ^{3}He/^{4}He ratios of $7.95R_A$ (van Soest at al. 1998) and 8.31–8.46 R_A (Pedroni et al. 1999), where R_A is the ^{3}He/^{4}He ratio in air, were obtained for the summit fumaroles of La Soufrière. These high values overlap with helium isotope ratios ($8 \pm 1R_A$) of mid-ocean ridge basalt (MORB) and indicate the significant presence of a mantle-derived component (van Soest at al. 1998; Pedroni et al. 1999). As anticipated, this isotopic evidence indicates that the summit fumaroles are fed by a peculiar zone of the underlying hydrothermal aquifer that receives a considerable input of fluids from a degassing magma body. However, the boiled-off water with an isotopically heavy magmatic signature was not detected elsewhere in the island, neither as a mixture with the main geothermal liquid nor by itself. It is unlikely that it totally boiled away in the dome area. Probably it has a small flux relative to that of meteorically derived geothermal fluids transferred through the volcano, so that the heavy isotopic signature is rapidly lost.

In addition to the fumarolic fields, several thermal springs are present around La Soufrière dome. Calcium–SO_4 thermal waters, produced through absorption of hydrothermal vapors in shallow groundwaters, are generally discharged from the springs closest to the active dome and at the highest elevations, whereas weakly thermal, conductively heated Ca–Na–HCO_3 springs are located at lower elevations and greater distances from the dome. Two thermal springs (Grosse Corde, Carbet) discharging Ca–Na–Cl waters are situated on the eastern slopes of La Soufrière dome. Chemical and isotopic evidence indicates that these Ca–Na–Cl waters are produced through mixing of shallow Ca–SO_4 waters and deep Na–Cl hydrothermal liquids.

The geographic distribution of the different thermal manifestations recognized in La Soufrière area suggests the presence of:

1. A central zone dominated by the ascent of steam, which is separated from a boiling hydrothermal aquifer and either discharges at the surface in fumarolic areas or is absorbed in shallow groundwaters
2. An outer zone, where the shallow groundwaters are heated through conduction or addition of Na–Cl liquids coming from hydrothermal aquifer(s).

The summit vents are likely located along a zone of high vertical permeability, such as a deep-reaching fracture or fault that might have acted as route of ascent for the magma that formed the dome. The deepest part of this permeable zone acts as a zone of preferential input of magmatic gases into the hydrothermal aquifer, and its shallowest part behaves as a zone of preferential discharge of the hydrothermal aquifer itself. However, magmatic fluids are prevented from forming the sort of magmatic gas column that passes across the hydrother-

mal aquifer and reaches the surface, as recognized at White Island (Giggenbach 1987) and Vulcano (Chiodini et al. 1995, and references therein). At Soufrière, either the flux of magmatic fluids entering the hydrothermal aquifer is not high enough, or the flux of hydrothermal fluids is sufficiently large, to substantially buffer the magmatic inflow. A situation similar to that of Soufrière was also observed at Monserrat before the eruption that started in 1995 (Chiodini et al. 1996), at Galeras (Fischer et al. 1997), and at Nevado del Ruiz (Giggenbach et al. 1990).

As for Galeras and Nevado del Ruiz, the reactivation of the system will probably be noticed by changes in fluid chemistry. At Galeras, fumarole chemistry became more hydrothermal prior to the eruption, due to a sealing process in the edifice. The eruptions, however, were driven by magmatic volatile input and accumulation in the system, resulting in pressure build up, as indicated by increases in the He content, the $^3He/^4He$ ratio, and the mantle fraction of C (Fischer et al. 1997; Sano et al. 1997).

Acknowledgements We thank J. Hernandez for logistic support, G. Hammouya, and R. Fellay, who helped us with part of the field work, and B. Christenson for comments and suggestions. We are indebted to B. Raco for the chemical analyses of the fumarolic fluids. We are grateful to T. Fischer and J. C. Varekamp for helpful comments on the first version of this manuscript.

References

Benauges S (1981) Etude géochimique et isotopique des eaux de rivières, sources froides et sources chaudes, aux abords du volcan de la Soufrière – Guadeloupe. Thèse 3e cycle, Univ Pierre et Marie Curie, Paris, pp 1–91

Berner EK, Berner RA (1996) Global environment: water, air, and geochemical cycles. Prentice Hall, Upper Saddle River, New Jersey, pp 1–376

Boudon G, Dagain J, Semet MP, Westercamp D (1987) Massif volcanique de la Soufrière Carte géologique et notice explicative 1/20,000, BRGM

Bouysse P, Westercamp D, Andreieff P, Baubron J-C, Scolari G (1985) Le volcanisme sous-marin Néogène récent au large des côtes Caraïbes des Antilles françaises. Relations avec le volcanisme à terre et évolution du front volcanique. Géol France 1:101–114

Chiodini G, Marini L (1998) Hydrothermal gas equilibria. I. The H_2O–H_2–CO_2–CO–CH_4 system. Geochim Cosmochim Acta 62:2673–2687

Chiodini G, Cioni R, Guidi M, Marini L (1991) Chemical geothermometry and geobarometry in hydrothermal aqueous solutions: a theoretical investigation based on a mineral-solution equilibrium model. Geochim Cosmochim Acta 55:2709–2727

Chiodini G, Cioni R, Leonis C, Marini L, Raco B (1993) Fluid geochemistry of Nisyros Island, Dodecanese, Greece. J Volcanol Geotherm Res 56:95–112

Chiodini G, Cioni R, Marini L, Panichi C (1995) Origin of the fumarolic fluids of Vulcano Island, Italy, and implications for volcanic surveillance. Bull Volcanol 57:99–110

Chiodini G, Cioni R, Frullani A, Guidi M, Marini L, Prati F, Raco B (1996) Fluid geochemistry of Montserrat Island, West Indies. Bull Volcanol 58:380–392

Cioni R, Corazza E (1981) Medium temperature fumarolic gas sampling. Bull Volcanol 44:23–29

Cioni R, Corazza E, Fratta M, Pescia A (1980) Sampling and analysis of medium-high temperature fumarolic gases. Bull PIRPSEV 31:14–22

Coplen TB (1988) Normalisation of oxygen and hydrogen isotope data. Chem Geol Isotope 72:293–297

Cormy G, Demians D'Archimbaud J, Surcin J (1970) Prospection géothermique aux Antilles Françaises, Guadeloupe et Martinique. Geothermics 2:57–72

D'Amore F, Panichi C (1980) Evaluation of deep temperature of hydrothermal systems by a new gas-geothermometer. Geochim Cosmochim Acta 44:549–556

Demians D'Archimbaud J, Surcin J (1972) Recherches géothermiques en Guadeloupe. Rev Géogr Phys Géol Dyn 14:211–228

Demians D'Archimbaud J, Surcin J (1976) Recherches d'énergie géothermique en Guadeloupe. Bull BRGM 4:365–373

Ellis AJ, Mahon WAJ (1977) Chemistry and geothermal systems. Academic Press, New York

Fischer TP, Sturchio NC, Stix J, Arehart GB, Counce D, Williams SN (1997) The chemical and isotopic composition of fumarolic gases and spring discharges from Galeras Volcano, Colombia. J Volcanol Geotherm Res 77:229–253

Fournier RO (1979a) Geochemical and hydrological considerations and the use of enthalpy-chloride diagrams in the predictions of underground conditions in hot-spring systems. J Volcanol Geotherm Res 5:1–16

Fournier RO (1979b) A revised equation for the Na/K geothermometer. Geotherm Resourc Council Trans 5:1–16

Fournier RO, Potter RW (1982) A revised and expanded silica (quartz) geothermometer. Geotherm Resourc Council Bull 11:3–12

Giggenbach WF (1987) Redox processes governing the chemistry of fumarolic gas discharges from White Island, New Zealand. Appl Geochem 2:143–161

Giggenbach WF (1988) Geothermal solute equilibria. Derivation of Na–K–Mg–Ca geoindicators. Geochim Cosmochim Acta 52:2749–2765

Giggenbach WF (1992a) Isotopic shifts in waters from geothermal and volcanic systems along convergent plate boundaries and their origin. Earth Planet Sci Lett 113:495–510

Giggenbach WF (1992b) Isotopic composition of geothermal water and steam discharges. In: Application of geochemistry in geothermal reservoir development (D'Amore F, co-ordinator), UNITAR-UNDP, pp 253–273

Giggenbach WF (1997) The origin and evolution of fluids in magmatic-hydrothermal systems. In: Barnes HL (eds) Geochemistry of hydrothermal ore deposits. Wiley, New York, pp 737–796

Giggenbach WF, Corrales Soto R (1992) Isotopic and chemical composition of water and steam discharges from volcanic–magmatic–hydrothermal systems of the Guanacaste Geothermal Province, Costa Rica. Appl Geochem 7:309–332

Giggenbach WF, Stewart MK (1982) Processes controlling the isotopic composition of steam and water discharges from steam vents and steam-heated pools in geothermal areas. Geothermics 11:71–80

Giggenbach WF, Garcia P, Londoño C, Rodriguez V, Rojas G, Calvache V (1990) The chemistry of fumarolic vapor and thermal spring discharges from the Nevado del Ruiz volcanic–magmatic–hydrothermal system, Colombia. J Volcanol Geotherm Res 42:13–39

Marini L, Agostini A, Cioni R, Guidi M, Leon O (1991) Guagua Pichincha volcano, Ecuador: fluid geochemistry in volcanic surveillance. J Volcanol Geotherm Res 46:21–35

Marini L, Principe C, Chiodini G, Cioni R, Fytikas M, Marinelli G (1993) Hydrothermal eruptions of Nisyros (Dodecanese, Greece). Past events and present hazard. J Volcanol Geotherm Res 56:71–94

Pascaline H (1980) Géochimie des roches et des eaux de sources chaudes du massif de la Soufrière de Guadeloupe, Petites Antilles. Thèse 3e cycle, Univ Paris Sud, Orsay, 150 pp

Pedroni A, Hammerschmidt K, Friedrichsen H (1999) He, Ne, Ar, and C isotope systematics of geothermal emanations in the Lesser Antilles Islands Arc. Geochim Cosmochim Acta 63:515–532

Reed MH (1997) Hydrothermal alteration and its relationship to ore fluid composition. In: Barnes HL (ed) Geochemistry of hydrothermal ore deposits. Wiley, New York, pp 517–611

Sano Y, Gamo T, Williams SN (1997) Secular variations of helium and carbon isotopes at Galeras volcano, Colombia. J Volcanol Geotherm Res 77:255–265

Traineau H, Sanjuan B, Beaufort D, Brach M, Castaing C, Correia H, Genter A, Herbrich B (1997) The Bouillante geothermal field (F.W.I.) revisited: new data on the fractured geothermal reservoir in light of a future stimulation experiment in a low productive well. Proc 22nd Workshop on Geothermal Reservoir Engineering, Stanford University, SGP-TR-155

Truesdell AH, Nathenson M, Rye RO (1977) The effects of subsurface boiling and dilution on the isotopic composition of Yellowstone thermal waters. J Geophys Res 82:3694–3704

Van Soest MC, Hilton DR, Kreulen R (1998) Tracing crustal and slab contributions to arc magmatism in the Lesser Antilles island arc using helium and carbon relationships in geothermal fluids. Geochim Cosmochim Acta 62:3323–3335

Westercamp D, Tazieff H (1980) Martinique, Guadeloupe, Saint-Martin, La Désirade, Guides géologiques régionaux. Masson, Paris

Wilson M (1989) Igneous petrogenesis. Unwin Hyman, London

Wolery TJ (1979) Calculation of chemical equilibrium between aqueous solutions and minerals: the EQ3/6 software package. Lawrence Livermore National Laboratory, Livermore

Wolery T (1992) EQ3NR, A computer program for geochemical aqueous speciation-solubility calculations: theoretical manual, user's guide and related documentation (version 7.0). Report UCRL-MA-110662, part III. Lawrence Livermore National Laboratory, Livermore

Wolery T, Daveler SA (1992) EQ6, A computer program for reaction path modeling of aqueous geochemical systems: theoretical manual, user's guide, and related documentation (version 7.0). Report UCRL-MA-110662, part IV. Lawrence Livermore National Laboratory, Livermore